

# Metallo-Hydrogel-Assisted Synthesis and Direct Writing of Transition Metal Dichalcogenides

Xining Zang,\* J. Nathan Hohman,\* Kaiyuan Yao, Penghong Ci, Aiming Yan, Minsong Wei, Takeshi Hayasaka, Alex Zettl, P. James Schuck, Junqiao Wu, and Liwei Lin\*

Two dimensional (2D) transition metal dichalcogenides (TMDCs) have attracted interest for their compelling nanoscale new properties and numerous potential applications including fast optoelectronic devices, ultrathin photovoltaics, and high-performance catalysts. Large-scale growth of uniform TMDC materials is essential for investigating their physics and for their integration into devices. However, the wafer scale deposition of TMDCs on arbitrary nonselective substrates is still beyond the current state-of-the-art. In this article, a method to synthesize layered TMDCs ( $\text{MoS}_2$  and  $\text{WS}_2$ ) at the wafer-scale by sulfurization of transition metal ions ( $\text{Mo}^{5+}$  and  $\text{W}^{6+}$ ) in a gelatin template (metallo-hydrogel) is reported. This process is adaptable to versatile substrates, including amorphous silicon oxide, high-temperature quartz, and silicon. Although the products are nominally few layer materials, direct band photoluminescent ( $\approx 1.8$  eV), similar to single- or decoupled multilayer  $\text{MoS}_2$  is observed. Finally, the solution-based deposition enables contact printing of TMDC channels to be useable for device applications including thin film transistors with printed silver contacts using the same process.

discovery of compelling electronic properties in graphene, a single layer of common graphite, sparked a “gold rush” in the search for interesting properties in other layered systems. The transition metal dichalcogenides (TMDCs) emerged as popular targets because of their intrinsic semiconducting phenomena enables their direct implementation in semiconductor devices.<sup>[3–6]</sup> Molybdenite, or  $\text{MoS}_2$ , which has been used as lubricant since the middle of last century,<sup>[7]</sup> has attracted particular interest because it transitions to a direct bandgap semiconductor in a single layer.<sup>[8–10]</sup> A variety of methods for preparing uniform and scalable TMDC films have been developed,<sup>[11,12]</sup> including chemical vapor deposition (CVD),<sup>[13–16]</sup> mechanical exfoliation,<sup>[17]</sup> and atomic layer deposition<sup>[18]</sup> (Table S1, Supporting Information). However, cost-effective large-area approaches with layer-number-control still

## 1. Introduction

2D materials are ultrathin, stable structures usually obtained by scaling down a layered material to a single layer.<sup>[1,2]</sup> The

remain challenging. Deposition of  $\text{MoS}_2$  and  $\text{WS}_2$  films on a nonepitaxial substrate (e.g.,  $\text{SiO}_2$ ) at the wafer scale has continued to be a significant challenge, and most strategies employ sophisticated and expensive metal organic CVD and yield

Dr. X. Zang  
Research Laboratory of Electronics  
Massachusetts Institute of Technology  
Cambridge, MA 02139, USA  
E-mail: xzang@mit.edu

Dr. X. Zang, K. Yao, Dr. M. Wei, T. Hayasaka, Prof. L. Lin  
Mechanical Engineering  
University of California Berkeley  
Berkeley, CA 94704, USA  
E-mail: lwlin@berkeley.edu

Dr. J. N. Hohman, Prof. P. J. Schuck  
Molecular Foundry  
Lawrence Berkeley National Laboratory  
Berkeley, CA 94720, USA  
E-mail: jnhoman@lbl.gov

K. Yao, Prof. P. J. Schuck  
Mechanical Engineering  
Columbia University  
New York City, NY 10027, USA

P. Ci, Prof. J. Wu  
Materials Science and Engineering  
University of California Berkeley  
Berkeley, CA 94704, USA

Dr. A. Yan, Prof. A. Zettl  
Physics Department  
University of California Berkeley  
Berkeley, CA 94704, USA

Dr. A. Yan, Prof. A. Zettl  
Material Science Division  
Lawrence Berkeley National Laboratory  
Berkeley, CA 94720, USA

Prof. A. Zettl  
Kavli Energy NanoSciences Institute at University of California Berkeley  
and Lawrence Berkeley National Laboratory  
Berkeley, CA 94720, USA

 The ORCID identification number(s) for the author(s) of this article can be found under <https://doi.org/10.1002/adfm.201807612>.

DOI: 10.1002/adfm.201807612

polycrystalline films with small domains.<sup>[19]</sup> Epitaxial CVD deposition of TMDC onto sapphire and mica substrates has been reported recently, although the substrate restriction requires inevitable transfer processes to further develop device applications.<sup>[20,21]</sup> Developing a solution process,<sup>[22]</sup> especially printing compatible process will be essential for large area synthesis and practical application of TMDC in electronic devices.<sup>[23]</sup>

Self-assembly is the autonomous organization of components into patterns or structures, which is a common feature in nature,<sup>[24]</sup> and principles of this concept are used increasingly in many disciplines.<sup>[25]</sup> Self-assembling lamellar surfactant templates have been used to produce 2D oxide materials<sup>[26,27]</sup> by restricting precursors to the interstices between lamella. The characteristics of the polymeric template superlattice can be varied by assembling them with over a range of concentrations of surfactant and solvent.<sup>[28]</sup> Recently, we reported the use of metal ions in gelatin hydrogels as a precursor for high-temperature synthesis of metal carbides. The gelatin is used as a sacrificial scaffold to impose lamellar organization of inorganic components with large interlayer spacings that is preserved after the thermal treatment.<sup>[29]</sup>

Here, we report a straightforward method to synthesize large-area TMDC films that express monolayer-like optoelectronic phenomena in a two-step process. First, we preorganize transition metal ions ( $\text{Mo}^{5+}$ ,  $\text{W}^{6+}$ ) into lamellar nanostructures using a gelatin-based hydrogel. This metallo-hydrogel can be spin-coated onto versatile substrates, including silicon oxide or high-temperature quartz. The metallo-hydrogel can then be converted to the corresponding TMDC ( $\text{MoS}_2$  and  $\text{WS}_2$ ) by annealing in sulfur vapor at 420 °C. By adjusting the concentration of surfactant and metal ions, TMDC films can be prepared in thicknesses ranging from few-layers to hundreds of nanometers. Despite the multilayered structures of the deposited materials, direct band photoluminescence at  $\approx 1.8$  and  $\approx 2.0$  eV is observed, and attributed to the A and B exciton, respectively. Interestingly, this is a property that is normally only observed in monolayer  $\text{MoS}_2$ , and is attributed to a surfactant-mediated decoupling of the  $\text{MoS}_2$  prepared by this approach. The scheme was then adapted to the direct writing and patterning of TMDC on versatile substrates using contact printing process, and we used these methods to prepare printed thin-film transistors using a  $\text{WS}_2$  channel, and silver source/drain contact electrodes. Such self-assembly assisted fabrication and patterning greatly increase the accessibility of TMDCs in commercial electronics and brings inspiration for other semiconducting materials manufacturing.

## 2. Results and Discussion

**Figure 1** depicts a schematic overview of the self-assembly and subsequent sulfurization scheme. We begin with the preparation of the metallo-hydrogel (Mo-gel and W-gel), the gelatin-based hydrogel with added molybdate or tungstate species, respectively. The bottom-up assembly of the gelatin template is shown schematically in Figure 1a–c. Self-assembling gelatin-based hydrogels can form large area membranes.<sup>[30]</sup> The ordering occurs in a layer-by-layer process that initiates at the air/liquid interface, a process resulting from convection-capillary forces

and recirculation flow generated by the Buoyancy–Marangoni effect.<sup>[31,32]</sup> Our objective was to identify a maximal loading of the metal species that would preserve the lamellar character of the hydrogel, and therefore conducted a study of how the concentrations of gelatin and  $\text{MoCl}_5$  impacted scaffold formation.

To ensure conformal spincoating and sulfurization performance, we first optimized the gelatin concentration and metal loading. We observed that concentration of 2 m (molal)  $\text{MoCl}_5$  and 10 wt% gelatin in DI water provide uniform and continuous films, as shown in the schematic overview of a silicon wafer spin-coated with the metal-containing hydrogel in Figure 1d. Mo-gels were prepared from initial gelatin solutions at 1%, 5%, 10%, and 20% by weight. Higher concentrations of gelatin led to cracking of the films, which led to poor film quality after sulfurization (**Figure 2a–d**). Excessive molybdate loading led to phase separation and precipitation of solid molybdenate species at the hydrogel interface (Figure 2a). We also investigated the addition of ethanol to promote convection during hydrogel formation, with the intention of increasing metal loading. However, this led to the unanticipated result of rapid evaporation of DI water/alcohol mixtures that generated bubbles during the subsequent sulfurization process and gave unacceptable uniformity (Figure 2d). We now consider the sulfurization of the metallo-hydrogel into the corresponding TMDC. The scanning electron microscopy (SEM) images in Figure 1d,g depict the featureless metallo-hydrogel template and its subsequent conversion into the layered TMDC. Sulfurization by elemental sulfur is performed at 420 °C for 30 min, converting the metallo-hydrogel to the corresponding TMDC (Figure 1e). Optical images reveal large-area films of lamellar TMDC after sulfurization (Figure 1f). Energy dispersion spectrum (EDS) mapping on such thin film indicate uniform homogenous  $\text{MoS}_2$  film, as shown in Figure S1 of the Supporting Information. EDS spectrum on a selected area of sample in Figure 1g is shown in Figure S2 of the Supporting Information. At substantially higher temperatures we found that metallic Mo began to grow, especially over 650 °C. Higher temperatures introduces crack and pinholes in the chalcogenide due to fierce decomposition of gel template.

Synchrotron X-ray microdiffraction and characterization results of a  $\text{MoS}_2$  film show millimeter-scale uniformity. The high-luminosity of the synchrotron X-ray source produced intense Laue patterns, a representative example shown in Figure 1h. Laue X-ray diffraction (XRD) results are shown in Figure 1h, indicating the overall crystalline nature of the film.<sup>[33]</sup> The orientation maps show variations of the out-of-plane orientation of up to 9.77° in the coarse map (Figure S3a, Supporting Information), while a smaller misalignment of 4.37° is resolved at high magnification (Figure S3b, Supporting Information). Such small out-of-plane titling indicates a relatively uniform structure with considerable coalignment. The high-resolution transmission electron microscopy images in Figure 1i–j depict a periodic atomically resolved crystalline lattice consistent with lattice spacings reported for  $\text{MoS}_2$ . The associated electron diffraction pattern in Figure 1i shows the characteristic hexagonal diffraction pattern of  $\text{MoS}_2$ , confirming the expected lattice spacing of 0.27 nm associated with the (100) plane of  $\text{MoS}_2$ . To study the local order of the product, a sample of TMDC was removed from the substrate onto a scotch tape backing.

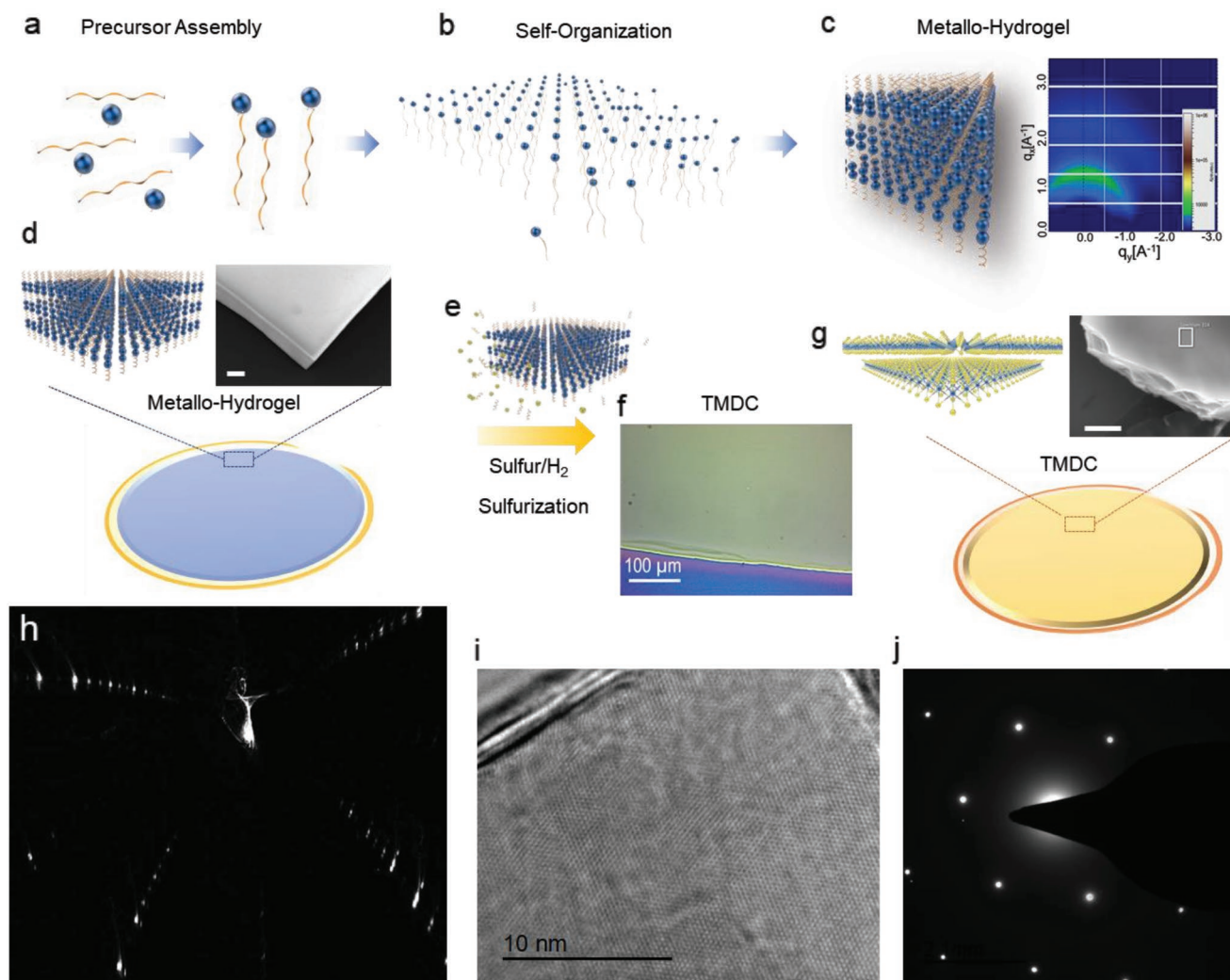


**Figure 1.** Self-assembly-assisted synthesis of TMDC. a) Transition metal ions (blue) coordinate functional groups in gelatin (orange helix). b) Phase-segregation tends to impose constituents into 2D lamellar structures. c) The mature metallo-hydrogel exhibits ordered structures of transition metal ions and a lamellar arrangement of gelatin chains as indicated by its grazing incident wide angle scattering. d) Metallo-hydrogel can be spin-coated onto wafers. Scale bar of as spin-coating film is 1  $\mu\text{m}$ . e) Chalcogenized by annealing in sulfur vapor converts metal ions into (f,g) TMDC while preserving the preorganization imposed by metallo-hydrogel formation. f) Optical image of as synthesized single crystalline large scale  $\text{MoS}_2$  thin film with a thickness of about 2  $\mu\text{m}$ . g) Inset: cross-section view scanning electron microscope image of (f), scale bar: 1  $\mu\text{m}$ . Energy dispersive X-ray spectroscopy (EDX) spectrum of selected area in (g) is shown in Figure S2 of the Supporting Information. h) Laue X-ray pattern mappings over a  $100 \times 100 \mu\text{m}^2$  area (step size  $5 \times 5 \mu\text{m}^2$ ) are aligned by zone-axis. The same set of Laue pattern indicate the single crystalline nature, while out-of-plane orientation map is shown in Figure S3 of the Supporting Information. Microdiffraction beamline 12.3.2 from the Advanced Light Source (ALS) at Lawrence Berkeley National Laboratory is employed. i) Transmission electron microscope (TEM) image of an exposed edge area of the  $\text{MoS}_2$  in (g), showing the 2D stacking structure and the honey-comb atomic structure of  $\text{MoS}_2$ . j) Diffraction pattern of (i).

Compared to other large crystalline semiconductor growth, this Mo-gel process presented here is fast and convenient (Table S1, Supporting Information).<sup>[34,35]</sup> The fast growth kinetics make it difficult to control the orientation and domain of TMDC in the polycrystalline films during the solution-based growth processes.<sup>[23,36,37]</sup> The advantage of the present work is to utilize gelatin as a template to assist the growth process for high quality films. Since the method was employed successfully to make thick (micrometer scale) TMDC deposits, we now turn to the development of few-layer TMDCs. To reduce the quantity of TMDC deposited, it was straightforward to dilute the Mo-gel solution; a 10 $\times$  dilution, for example, yielded a 0.2 m

$\text{MoCl}_5$  solution with 1% gelatin. After setting, this film could be chalcogenized to produce TMDCs in the 10–100 nm range. Figures S2e–g and S4 of the Supporting Information include more detail on samples in this category. Unlike the thicker TMDC compounds formed above, dilute gelatin templates tended to yield separated TMDC islands. TMDC crystals exhibit central nucleation sites and radial growth patterns, indicating a nonequilibrium growth process linked to the surface tension mismatch (Figure 2e–h).<sup>[38]</sup> X-ray photoelectron spectroscopy (XPS) in Figure S3c of the Supporting Information shows a sulfur deficient composition of S:Mo (1.85:1). We therefore tested the use of surfactants to reduce the surface tension

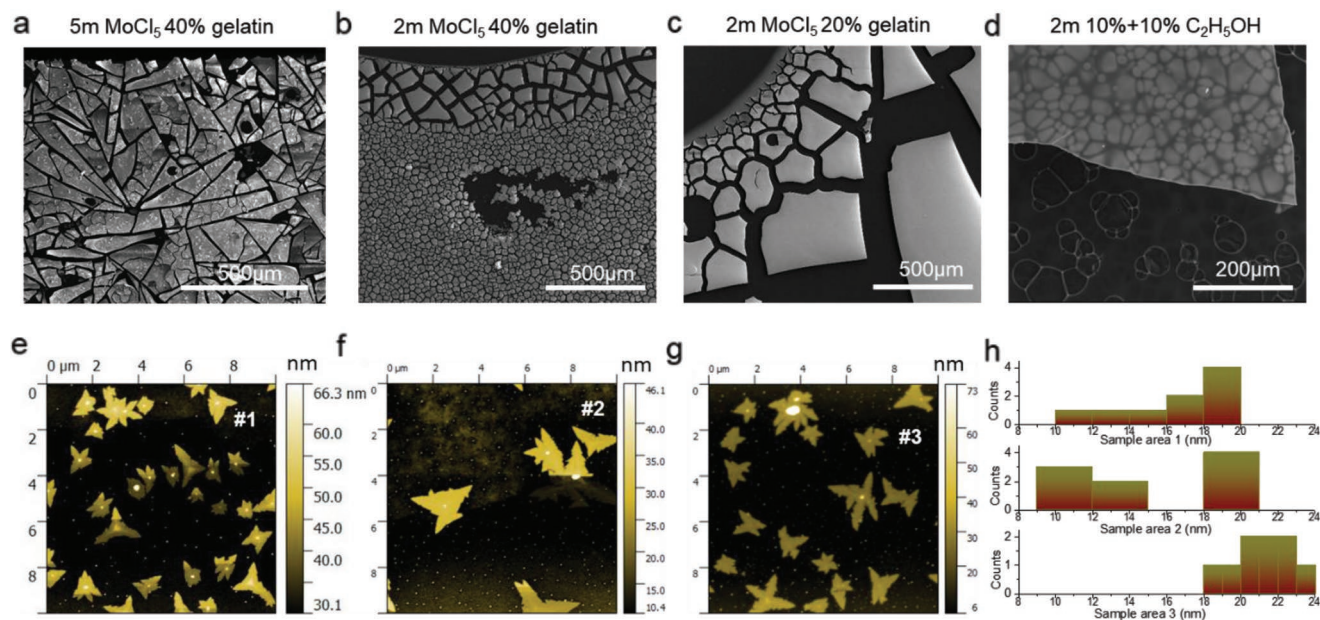


**Figure 2.** MoS<sub>2</sub> thin film derived with Mo-gel precursor with different concentrations. a) SEM image of cracked MoS<sub>2</sub> with lots of particles desorbed on surface grown from spin-coated Mo-gel precursor with concentration of 5 m Mo<sup>5+</sup> and 40% gelatin. b) SEM image of cracked MoS<sub>2</sub> grown from spin-coated Mo-gel precursor with concentration of 2 m Mo<sup>5+</sup> and 40% gelatin. c) SEM image of more continuous MoS<sub>2</sub> grown from spin-coated Mo-gel precursor with concentration of 2 m Mo<sup>5+</sup> and 20% gelatin. d) SEM image of larger continuous MoS<sub>2</sub> grown from Mo-gel precursor with concentration of 2 m Mo<sup>5+</sup>, 20% gelatin, and 20% alcohol in solvent. e–g) AFM mapping of as grown MoS<sub>2</sub> showing radial growing patterns, using diluted Mo-gel. (f) Statistical results of different domain thickness in (e–g).

and improve the nucleation and growth parameters of the deposited TMDC materials. Sodium dodecyl benzene sulfonate (SDBS) was added to the solution to decrease the surface tension, and enable the precursors to form TMDCs at the mono-to-few layer thicknesses. Because this surfactant is well known to form micelles at high concentrations, selected a concentration below the critical micelle concentration of 10<sup>-4</sup> m.<sup>[39]</sup> We observed that low concentrations of Mo-gel (Mo<sup>5+</sup> 10<sup>-3</sup> m 1% gelatin 10<sup>-4</sup> m SDBS in DI water) and W-gel (W<sup>6+</sup> 10<sup>-3</sup> m 1% gelatin 10<sup>-4</sup> m SDBS in *N*-methyl-2-pyrrolidone (NMP)) solutions yield small flakes of MoS<sub>2</sub> and WS<sub>2</sub>, respectively, with the characteristic triangular shapes of single crystal structures. With the same metal ion and gelatin concentration, an increase of SDBS concentration will change the morphology of TMDC to nanowires/nanotubes (Figure S5a,d, Supporting Information).

**Figure 3** collects SEM images and synchrotron grazing-incidence wide-angle X-ray scattering (GIWAXS) results for thin films of WS<sub>2</sub> and MoS<sub>2</sub>. The GIWAXS results reveal characteristic signatures of the TMDC films, most notably the position and spacing in *q* space of the basal plane of the TMDC compounds. Strong reflections attributed to the (001) plane of the material are evident, attributed to the preferred orientation of the crystals cofacial to the substrate. The presence of these characteristic reflections confirms the identity of the product and the crystalline order of the nanostructured thin films. The preferred orientation of the crystallites on the substrate is evident in both the images and in the diffraction data. No other preferred orientation shows sharp and obvious spot, while the circles attributed to other lattice plane indicate the stacking of layers are disordered in the basal plane (Figure 3c,d,g,h).

Next, we probed the optical response of the thin films of TMDC. Layered self-assembled MoS<sub>2</sub> exhibit major photoluminescence (PL) at ≈1.8 eV and a minor peak at ≈1.95 eV (A,B excitations) (Figure 3d; Figure S5c, Supporting Information), similar to the direct-gap exciton seen in monolayer systems.<sup>[40]</sup> Meanwhile, the indirect bandgap PL peak normally observed at 1.3 eV<sup>[41]</sup> does not show up, in Figure S5f of the Supporting Information. Since this direct-gap PL results only occur in monolayer or intercalated structures,<sup>[42,43]</sup> it implies the fabricated films are isolated monolayers in the form of a “bulk” layered structure. We hypothesize that this could originate from two possible structural motifs: (a) the surfactant residuals decouple the MoS<sub>2</sub> layers resulting in monolayer-like optical properties and (b) twisted interlayer orientation in the *x*–*y* plane (Figure 2c,g) induces potential larger interlayer distance and weaker interlayer coupling due to steric effects.<sup>[44]</sup> Considering a randomly oriented stacking (Figure 3c,d,g,h), the real scenario should be much more complicated. The solution process decouples the interlayer stacking, making each layer more “isolated” and able to exhibit some monolayer-like emission. This phenomenon has been previously reported in ReS<sub>2</sub> wherein the composite layers are decoupled electronically and therefore perform as direct-gap semiconductors.<sup>[45]</sup> Further details of the optical properties of the thin films of TMDC are shown in Figure S5 of the Supporting Information.

The relatively low-temperature sulfurization process further enables TMDC fabrication on many other platforms such as temperature resilient polymers for possible broad applications in flexible electronics. First, we show the feasibility to use the gelatin/ion solutions as the inks and directly write the word

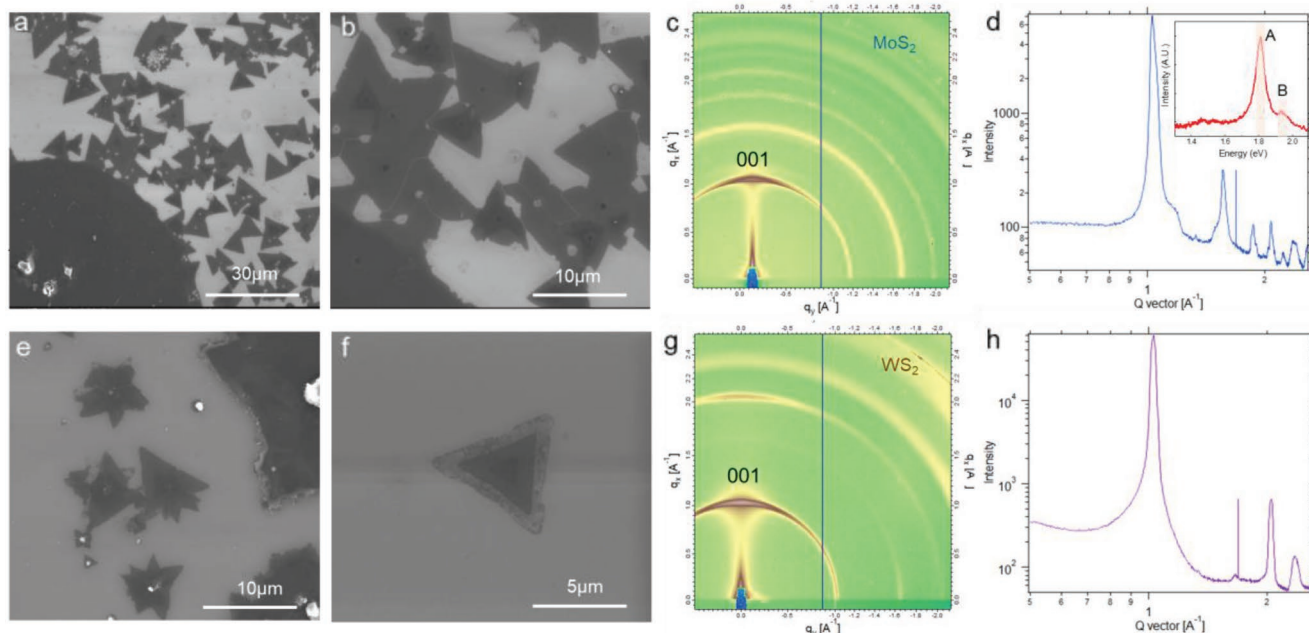


**Figure 3.** Multiple layer MoS<sub>2</sub> and WS<sub>2</sub> using lower concentration ion-gel-SDBS precursor. a,b) SEM images of MoS<sub>2</sub>. c) Grazing incident wide angle X-ray diffraction pattern of (a) and (b) showing strong preferred (001) orientation. d) 1D spectrum integrated from (c). Inset: photoluminescence (PL) of MoS<sub>2</sub> in (a) and (b). e–f) Multiple layer WS<sub>2</sub> via lower concentration W-gel-SDBS precursor. (e,f) SEM images of few layer WS<sub>2</sub>. g) Grazing incident wide angle X-ray diffraction pattern of (e) and (f) showing strong preferred (001) orientation. h) 1D spectrum integrated from (g).

“Cal” by hand onto substrates as shown in Figure 4a. The Raman mapping of the written feature is shown in Figure 4a and Figure S7 (Supporting Information). Raman map of the two peaks ( $E_{2g}^1$  and  $A_{1g}$ ) distance of the written sample shows a range from 22 to 25  $\text{cm}^{-1}$ , mostly 24 to 25  $\text{cm}^{-1}$ . The thickness should be around 6–7 layers.<sup>[46,47]</sup> In Figure 4b, the ion-gel ink is utilized with a syringe needle for the printing process. The setup includes a X–Y stage to control the lateral deposition positions, and a z-directional actuator to control the gap between the syringe head and the substrate. A printing syringe is connected to a pump for the Mo/W ink supply in a controlled chamber for stable temperature and humidity. The linewidth of printed feature is  $\approx 100 \mu\text{m}$ , showing the uniform edge of TMDC film derived from the precursor with low-concentration SDBS. Some deposition results using the optimized parameters are demonstrated to grow the ultrathin 2D MoS<sub>2</sub> and WS<sub>2</sub> as shown in Figure 4c, respectively. As shown from the Raman spectra in Figure 4c,  $E_{2g}^1$  peak at  $\approx 380 \text{ cm}^{-1}$  and interlayer vibration  $A_{1g}$  peak at  $\approx 405 \text{ cm}^{-1}$  indicate few layers of MoS<sub>2</sub>, the distance of  $\approx 25 \text{ cm}^{-1}$  indicates few layers of MoS<sub>2</sub>.<sup>[46]</sup>  $E_{2g}^1$  peak at  $\approx 353 \text{ cm}^{-1}$  and inter-layer vibration  $A_{1g}$  peak at  $\approx 420 \text{ cm}^{-1}$  result a distance of  $\approx 67 \text{ cm}^{-1}$  indicate few layers of WS<sub>2</sub>.<sup>[48]</sup> Atomic force microscopy (AFM) mapping is shown in Figure S8 of the Supporting Information. The thickness of the printed feature is around 7 nm. XPS results in Figure S9 of the Supporting Information confirm the elemental composition of the as-printed MoS<sub>2</sub> and WS<sub>2</sub>. GIWAXS scattering data of printed films also reveal the expected (Figure S10, Supporting Information) (001) reflection of the crystals, with preferred z-direction orientation and disordered stacking orientation.

The printing process can be deployed for the wafer scale patterning of TMDC channels suitable for device architectures (Figure 4d). We use a previously reported Ag-gelatin precursor in the same contact set up, which is reduced to silver electrode after annealing at 300 °C (Figure 4d).<sup>[30]</sup> Silver ink (6 m Ag<sup>+</sup> and 60% gelatin) is utilized to fabricate source and drain contacts as well as interconnects, enabling preparation of a printed thin film transistor TFT array devices are shown in Figure 4d, and employ the printed MoS<sub>2</sub> or WS<sub>2</sub> as channel materials on a silicon substrate with silicon dioxide as the gate oxide material. We selected the WS<sub>2</sub> over the MoS<sub>2</sub> for that device preparation since it is predicted to have better performance from previous theoretical and experimental work.<sup>[49,50]</sup> The measurement results based on the WS<sub>2</sub> channels (200  $\mu\text{m} \times 100 \mu\text{m}$ ) are shown in Figure 4e,f, Figure S12 and Table S2 (Supporting Information), for the drain current ( $I_d$ ) versus drain voltage ( $V_d$ ) and,  $I_d$  versus  $V_g$  curves, respectively.  $V_g$  is the gate voltage. The drain current is tuned from  $10^{-10}$  to  $10^{-6}$  A, indicating an on–off ratio on the order of  $10^4$ . We estimate the field effect mobility from the linear region with in the range of 30–50  $\text{cm}^2 \text{ V}^{-1} \text{ s}^{-1}$  (Figure S12, Table S2, Supporting Information), using the equation  $\mu_{FE} = (dI_d/dV_g)/(C_{ox}V_{ds}W/L)$ . The gate oxide capacitance ( $C_{ox}$ ) of the 285 nm SiO<sub>2</sub> dielectric layer is  $\approx 1.2 \times 10^{-4} \text{ F m}^{-2}$ , and  $W/L$  is the width to length ratio of WS<sub>2</sub> channel. Such mobility is consistent with air-exposed WS<sub>2</sub> thin film transistors, which are generally  $<100 \text{ cm}^2 \text{ V}^{-1} \text{ s}^{-1}$  at room temperature,<sup>[51–54]</sup> and could be improved by optimizing the device structure and packing.<sup>[55]</sup> The presence of amorphous carbon observed in Raman spectra (Figure S11, Supporting Information) can affect the electronic properties and device performances and may introduce noise and the off-current problems (Figure S12, Supporting Information).

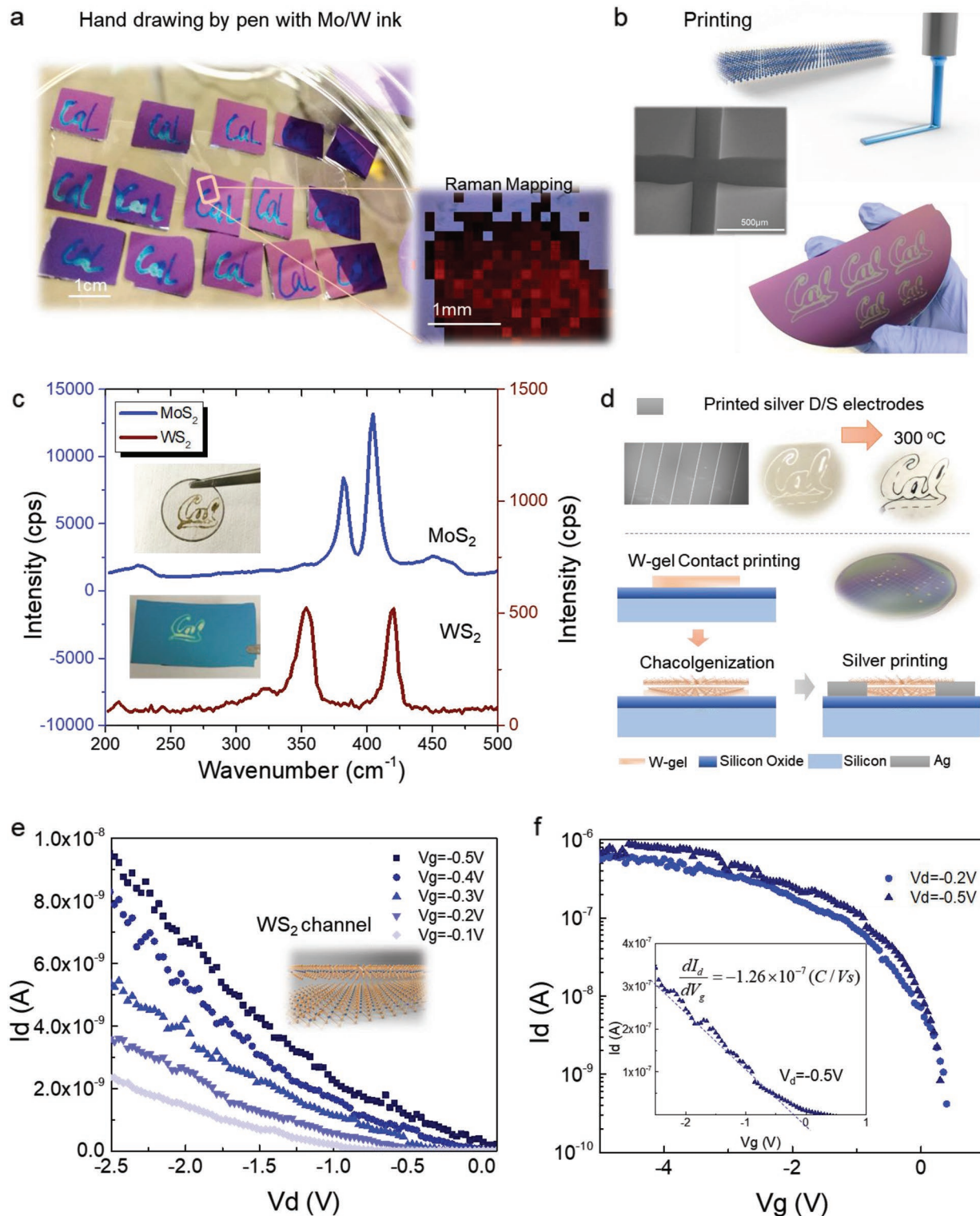


**Figure 4.** Printing-based TMDC deposition on versatile substrates. a) Writing “cal” with a pen filled with Mo/W ink onto silicon oxide and sulfurized to TMDC. Inset is Raman mapping of a selected area of as-written MoS<sub>2</sub> on silicon oxide. b) Precisely printed calligraphy via computer aid designing (CAD) tools. c) Raman spectroscopy of printed MoS<sub>2</sub> and WS<sub>2</sub>, showing typical peaks coherent with multiplayer MoS<sub>2</sub> and WS<sub>2</sub>. d) Fabrication process of direct-write TMDC transistors on a 4 in. silicon wafer. Thin film transistors (TFTs) using the direct-write TMDC films as the channel materials and direct-write silver films as the source, drain, and electrical interconnects on top of a silicon wafer. Silver-gelatin ink is employed for the direct-write Ag electrodes and interconnects.<sup>[30]</sup> e) The  $I_d$  $V_d$  curves and f) the  $I_d$  $V_g$  curves of an as printed WS<sub>2</sub> TFT with gate voltage from -0.2 to -0.5 V using direct-write silver electrodes as source and drain.

### 3. Conclusion

In this article, we presented a self-assembly-assisted solution process for large-area TMDC synthesis using a metallo-hydrogel as a sacrificial precursor. By systematically controlling the transition metal ion concentration, hydrogel concentration, surfactant concentration, and solvent properties, we optimized conditions to grow multilayered stacks of TMDCs with uniform morphology. We also demonstrated that films prepared in this way exhibit intriguing optical properties that mostly exist in monolayer-like materials rather than bulk TMDC, which are hypothetically induced by rotational disorder of crystalline planes and interstitial surfactant molecules that decouples the layers. Furthermore, this multilayered growth method also enables direct writing of TMDC on versatile substrates (silicon oxide, quartz) with contact printing set up, which can be used immediately for the batch fabrication of TMDC-based electronic devices such as thin-film transistors. Such processing is not only limited to the use in TMDC growth, but could be generalized for other semiconducting materials (GaN, InP, etc.) with design of precursors. Combine the printing process in additive manufacturing, TMDC-based superlattice,<sup>[43,56]</sup> heterostructures<sup>[57–59]</sup> using a “rainbow jelly” (a gelatin desert based on differently flavored gelatins) format.<sup>[60,61]</sup> By spin-coating and curing metallo-hydrogels with different metals and subsequently chalcogenizing the stack, new compositional, structural, and optoelectronic properties could be exploited in such vertically integrated heterostructures.

### 4. Experimental Section

**Materials:** Molybdenum pentachloride (>99.9% wt), gelatin (derived from porcine skin), ammonium molybdate (>95% wt), sulfur powder, SDBS, tungsten hexachloride (>99.9% wt), and NMP were used as received from Sigma-Aldrich (St. Louis, MO). n-Type silicon wafers and silicon wafers with 285 nm thermal oxide were used as received from University Wafers.

**Methods: Metallo-Hydrogel Ink/Precursor Preparation:**  $\text{Mo}^{5+}$ -Gel Preparation: Molybdenum pentachloride was dissolved in DI water to make 2 M solution. High concentration  $\text{Mo}^{5+}$  solution was presented using mass molarity, since it did not follow the dilution solution and mass molarity simplified the quantitative evaluation. However, down to 0.1 M and  $10^{-4}$  M per kg solvent the mass molarity was almost the same as volume molarity. In this paper, mass molarity was employed for consistency. Gelatin was dissolved in  $\text{MoCl}_5$  solutions to make concentrations of 1%, 5%, 10%, and 20% by weight of solvent (DI water). The Mo-gel solution was spin-coated onto silicon with 285 nm silicon oxide at a speed of 4000 rpm. Smaller concentrations were employed for preparing layered  $\text{MoS}_2$  films. SDBS surfactant was employed for films targeting few-layered  $\text{MoS}_2$ . Gelatin and  $\text{Mo}^{5+}$  concentration were diluted to 0.1% and 0.1 M for mono-few layer self-assembly. Spin-coating rate was increased to 6000 rpm for thin samples.

**$\text{W}^{6+}$ -Gel Preparation:**  $\text{WCl}_6$  was dissolved in NMP to achieve a concentration of 0.1 M with gelatin concentration of 0.1 wt%. SDBS with a concentration of  $10^{-4}$  M was added to W-NMP solution to make the printing precursor.

**Chalcogenide Conversion and Template Removal:** Sulfur annealing was performed at 420 °C in Thermal Lab 1 zone furnace, with a distance between sulfur powder and predecorated substrates of 5 cm.  $\text{N}_2$  or Ar carrier gasses were used with a flow rate of 30 sccm. The growing results using 5 sccm  $\text{H}_2$  with  $\text{N}_2$  were compared with those with pure  $\text{N}_2$  flow, which is quite similar. A 15 min temperature ramp, and the samples were then held at 420 °C for 30 min. KOH solution was used to wash

the waste gas at the end of flow system. After the furnace was cooled to room temperature, samples were transferred onto hot plate at 420 °C for 1 h to remove the residual gelatin.

**Characterization and Analysis:** Optical microscopy (Keyence 600), SEM (FEI Quanta 3D), and TEM (FEI Tecnai) were employed to study the morphology and the structure of as-grown and transferred  $\text{MoS}_2$ .  $\text{MoS}_2$  film was peeled and transferred onto scotch tape or a copper TEM grid for microdiffraction XRD or TEM analysis, respectively. XRD (Bruker D8) and single crystal XRD (Advanced Light Source, ALS, microdiffraction beamline 12.3.2) were employed to study the crystallinity of  $\text{MoS}_2$ . The sample was transferred onto scotch tape to avoid background from silicon wafer and scanned a  $100 \mu\text{m} \times 100 \mu\text{m}$  area with a step of 5  $\mu\text{m}$ . The 400 Laue diffraction patterns were merged to zone axis all as (002), and to resolve the out-of-plane deviation in the film. Raman spectrum (Renishaw inVia) and AFM were used to observe the stacking layers  $\text{MoS}_2$ .

**TFT Printing and Characterization:**  $\text{W}^{6+}$ -gel-SDBS ink was deposited on silicon oxide substrate using a set with an X–Y stage to control the lateral deposition positions in and a z-directional actuator to control the gap between the syringe head and the substrate. Patterned W ion precursor was sulfurized as the channel. Source and drain contacts were printed using silver acetate-gelatin (6 M, 60% in deionized water) solution, which was anneal in air for 30 min at 300 °C.<sup>[80]</sup> Semiconductor analyzer (Agilent Technology) integrated with a probe station (Lakeshore TTPX) was used to test the  $I_d$ – $V_g$  and  $I_d$ – $V_d$  curves, with back gate voltage added to the silicon substrate beneath silicon oxide.

### Supporting Information

Supporting Information is available from the Wiley Online Library or from the author.

### Acknowledgements

Work at the Molecular Foundry, beamlines 12.3.2 and 7.3.3 at the Advanced Light Source, was supported by the Office of Science, Office of Basic Energy Sciences, of the U.S. Department of Energy under Contract No. DE-AC02-05CH11231. This work was supported in part by the Director, Office of Science, Office of Basic Energy Sciences, Materials Sciences and Engineering Division, of the U.S. Department of Energy under Contract No. DE-AC02-05CH11231, within the van der Waals Heterostructures Program (KCWF16), which provided for PL measurements, and within the sp<sup>2</sup>-Bonded Materials Program (KC2207), which provided for Raman measurements. The authors thank Prof. Tsu-Jae King-Liu in the Electrical Engineering and Computer Science Department of UC Berkeley for sharing the analyzers for TFT device measurement and Prof. Xiaolong Zou at the Tsinghua-Berkeley Shenzhen Institute for the discussions on the DFT simulation of  $\text{MoS}_2$  band structure. The microdiffraction pattern was conducted with the help of Dr. Nobumichi Tamura, and the GIWAX was conducted with the help of Dr. Chenhui Zhu at the Advanced Light Source (ALS) at Lawrence Berkeley National Laboratory.

### Conflict of Interest

The authors declare no conflict of interest.

### Keywords

contact printing, self-assembly, thin film transistor (TFT) array, transition metal dichalcogenide (TMDC)

Received: October 28, 2018  
Revised: April 5, 2019  
Published online: May 9, 2019

- [1] R. Suzuki, M. Sakano, Y. J. Zhang, R. Akashi, D. Morikawa, A. Harasawa, K. Yaji, K. Kuroda, K. Miyamoto, T. Okuda, K. Ishizaka, R. Arita, Y. Iwasa, *Nat. Nanotechnol.* **2014**, *9*, 611.
- [2] G. R. Bhimanapati, Z. Lin, V. Meunier, Y. Jung, J. Cha, S. Das, D. Xiao, Y. Son, M. S. Strano, V. R. Cooper, L. B. Liang, S. G. Louie, E. Ringe, W. Zhou, S. S. Kim, R. R. Naik, B. G. Sumpter, H. Terrones, F. N. Xia, Y. L. Wang, J. Zhu, D. Akinwande, N. Alem, J. A. Schuller, R. E. Schaak, M. Terrones, J. A. Robinson, *ACS Nano* **2015**, *9*, 11509.
- [3] E. A. Schriber, D. C. Poppo, M. Yeung, M. A. Brady, S. Corlett, J. N. Hohman, *ACS Appl. Nano Mater.* **2018**, *1*, 3498.
- [4] S. Z. Butler, S. M. Hollen, L. Y. Cao, Y. Cui, J. A. Gupta, H. R. Gutierrez, T. F. Heinz, S. S. Hong, J. X. Huang, A. F. Ismach, E. Johnston-Halperin, M. Kuno, V. V. Plashnitsa, R. D. Robinson, R. S. Ruoff, S. Salahuddin, J. Shan, L. Shi, M. G. Spencer, M. Terrones, W. Windl, J. E. Goldberger, *ACS Nano* **2013**, *7*, 2898.
- [5] H. Wang, L. L. Yu, Y. H. Lee, Y. M. Shi, A. Hsu, M. L. Chin, L. J. Li, M. Dubey, J. Kong, T. Palacios, *Nano Lett.* **2012**, *12*, 4674.
- [6] A. Nourbakhsh, A. Zubair, R. N. Sajjad, K. G. A. Tavakkoli, W. Chen, S. Fang, X. Ling, J. Kong, M. S. Dresselhaus, E. Kaxiras, K. K. Berggren, D. Antoniadis, T. Palacios, *Nano Lett.* **2016**, *16*, 7798.
- [7] R. I. Christy, *Thin Solid Films* **1980**, *73*, 299.
- [8] M. Amani, R. A. Burke, X. Ji, P. Zhao, D. H. Lien, P. Taheri, G. H. Ahn, D. Kirya, J. W. Ager, E. Yablonovitch, J. Kong, M. Dubey, A. Jaye, *ACS Nano* **2016**, *10*, 6535.
- [9] K. Wang, K. De Greve, L. A. Jauregui, A. Sushko, A. High, Y. Zhou, G. Scuri, T. Taniguchi, K. Watanabe, M. D. Lukin, H. Park, P. Kim, *Nat. Nanotechnol.* **2018**, *13*, 128.
- [10] X. X. Zhang, T. Cao, Z. G. Lu, Y. C. Lin, F. Zhang, Y. Wang, Z. Q. Li, J. C. Hone, J. A. Robinson, D. Smirnov, S. G. Louie, T. F. Heinz, *Nat. Nanotechnol.* **2017**, *12*, 883.
- [11] H. T. Wang, H. T. Yuan, S. S. Hong, Y. B. Li, Y. Cui, *Chem. Soc. Rev.* **2015**, *44*, 2664.
- [12] X. Ling, Y. X. Lin, Q. Ma, Z. Q. Wang, Y. Song, L. L. Yu, S. X. Huang, W. J. Fang, X. Zhang, A. L. Hsu, Y. Q. Bie, Y. H. Lee, Y. M. Zhu, L. J. Wu, J. Li, P. Jarillo-Herrero, M. Dresselhaus, T. Palacios, J. Kong, *Adv. Mater.* **2016**, *28*, 2322.
- [13] Y. H. Lee, X. Q. Zhang, W. J. Zhang, M. T. Chang, C. T. Lin, K. D. Chang, Y. C. Yu, J. T. W. Wang, C. S. Chang, L. J. Li, T. W. Lin, *Adv. Mater.* **2012**, *24*, 2320.
- [14] Q. Q. Ji, Y. F. Zhang, T. Gao, Y. Zhang, D. L. Ma, M. X. Liu, Y. B. Chen, X. F. Qiao, P. H. Tan, M. Kan, J. Feng, Q. Sun, Z. F. Liu, *Nano Lett.* **2013**, *13*, 3870.
- [15] Y. F. Yu, C. Li, Y. Liu, L. Q. Su, Y. Zhang, L. Y. Cao, *Sci. Rep.* **2013**, *3*, 1866.
- [16] W. Chen, J. Zhao, J. Zhang, L. Gu, Z. Z. Yang, X. M. Li, H. Yu, X. T. Zhu, R. Yang, D. X. Shi, X. C. Lin, J. D. Guo, X. D. Bai, G. Y. Zhang, *J. Am. Chem. Soc.* **2015**, *137*, 15632.
- [17] B. Radisavljevic, A. Radenovic, J. Brivio, V. Giacometti, A. Kis, *Nat. Nanotechnol.* **2011**, *6*, 147.
- [18] X. Zang, C. Shen, E. Kao, R. Warren, R. Zhang, K. S. Teh, J. Zhong, M. Wei, B. Li, Y. Chu, M. Sanghadasa, A. Schwartzberg, L. Lin, *Adv. Mater.* **2018**, *30*, 1704754.
- [19] K. Kang, S. Xie, L. Huang, Y. Han, P. Y. Huang, K. F. Mak, C.-J. Kim, D. Muller, J. Park, *Nature* **2015**, *520*, 656.
- [20] D. Dumcenco, D. Ovchinnikov, K. Marinov, P. Lazić, M. Gibertini, N. Marzari, O. L. Sanchez, Y.-C. Kung, D. Krasnozhan, M.-W. Chen, S. Bertolazzi, P. Gillet, A. Fontcuberta i Morral, A. Radenovic, A. Kis, *ACS Nano* **2015**, *9*, 4611.
- [21] H. Yu, M. Z. Liao, W. J. Zhao, G. D. Liu, X. J. Zhou, Z. Wei, X. Z. Xu, K. H. Liu, Z. H. Hu, K. Deng, S. Y. Zhou, J. A. Shi, L. Gu, C. Shen, T. T. Zhang, L. J. Du, L. Xie, J. Q. Zhu, W. Chen, R. Yang, D. X. Shi, G. Y. Zhang, *ACS Nano* **2017**, *11*, 12001.
- [22] A. S. George, Z. Mutlu, R. Ionescu, R. J. Wu, J. S. Jeong, H. H. Bay, Y. Chai, K. A. Mkhoyan, M. Ozkan, C. S. Ozkan, *Adv. Funct. Mater.* **2014**, *24*, 7461.
- [23] R. Ionescu, B. Campbell, R. Wu, E. Aytan, A. Patalano, I. Ruiz, S. W. Howell, A. E. McDonald, T. E. Beechem, K. A. Mkhoyan, M. Ozkan, C. S. Ozkan, *Sci. Rep.* **2017**, *7*, 6419.
- [24] G. M. Whitesides, B. Grzybowski, *Science* **2002**, *295*, 2418.
- [25] S. Mann, *Nat. Mater.* **2009**, *8*, 781.
- [26] Z. Sun, T. Liao, Y. Dou, S. M. Hwang, M.-S. Park, L. Jiang, J. H. Kim, S. X. Dou, *Nat. Commun.* **2014**, *5*, 3813.
- [27] L. L. Peng, P. Xiong, L. Ma, Y. F. Yuan, Y. Zhu, D. H. Chen, X. Y. Luo, J. Lu, K. Amine, G. H. Yu, *Nat. Commun.* **2017**, *8*, 15139.
- [28] M. Ballauff, *Science* **2016**, *352*, 656.
- [29] X. Zang, C. Shen, Y. Chu, B. Li, M. Wei, J. Zhong, M. Sanghadasa, L. Lin, *Adv. Mater.* **2018**, *30*, 1800062.
- [30] H. Jang, B. Seong, X. Zang, H. Lee, J. W. Bae, D. Cho, E. Kao, C. Yang, G. Kang, Y. Liu, H. S. Park, D. Byun, L. Lin, *Adv. Mater. Interfaces* **2018**, *5*, 1701491.
- [31] E. Balliu, H. Anderson, M. Engholm, R. Zhang, S. Forsberg, H. Olin, *Proc. SPIE* **2016**, *9736*.
- [32] V. I. Uricanu, M. H. G. Duits, D. Filip, R. M. F. Nelissen, W. G. M. Agterof, *J. Colloid Interface Sci.* **2006**, *298*, 920.
- [33] J. McCollum, M. L. Pantoya, N. Tamura, *Acta Mater.* **2016**, *103*, 495.
- [34] Y. B. Zhou, B. Deng, Y. Zhou, X. B. Ren, J. B. Yin, C. H. Jin, Z. F. Liu, H. L. Peng, *Nano Lett.* **2016**, *16*, 2103.
- [35] V. Zolyomi, N. D. Drummond, V. I. Fal'ko, *Phys. Rev. B* **2013**, *87*, 195403.
- [36] M. V. Nardi, M. Timpel, G. Ligorio, N. Z. Morales, A. Chiappini, T. Toccoli, R. Verucchi, R. Ceccato, L. Pasquali, E. J. W. List-Kratochvil, A. Quaranta, S. Dire, *ACS Appl. Mater. Interfaces* **2018**, *10*, 34392.
- [37] X. Y. Yu, M. S. Prevot, K. Sivula, *Chem. Mater.* **2014**, *26*, 5892.
- [38] C. X. Cong, J. Z. Shang, X. Wu, B. C. Cao, N. Peimyooc, C. Qiu, L. T. Sun, T. Yu, *Adv. Opt. Mater.* **2014**, *2*, 131.
- [39] S. K. Hait, P. R. Majhi, A. Blume, S. P. Moulik, *J. Phys. Chem. B* **2003**, *107*, 3650.
- [40] A. Splendiani, L. Sun, Y. B. Zhang, T. S. Li, J. Kim, C. Y. Chim, G. Galli, F. Wang, *Nano Lett.* **2010**, *10*, 1271.
- [41] A. Steinhoff, J. H. Kim, F. Jahnke, M. Rösner, D. S. Kim, C. Lee, G. H. Han, M. S. Jeong, T. O. Wehling, C. Gies, *Nano Lett.* **2015**, *15*, 6841.
- [42] Y. Jung, Y. Zhou, J. J. Cha, *Inorg. Chem. Front.* **2016**, *3*, 452.
- [43] C. Wang, Q. Y. He, U. Halim, Y. Y. Liu, E. B. Zhu, Z. Y. Lin, H. Xiao, X. D. Duan, Z. Y. Feng, R. Cheng, N. O. Weiss, G. J. Ye, Y. C. Huang, H. Wu, H. C. Cheng, I. Shakir, L. Liao, X. H. Chen, W. A. Goddard, Y. Huang, X. F. Duan, *Nature* **2018**, *555*, 231.
- [44] K. H. Liu, L. M. Zhang, T. Cao, C. H. Jin, D. A. Qiu, Q. Zhou, A. Zettl, P. D. Yang, S. G. Louie, F. Wang, *Nat. Commun.* **2014**, *5*, 4966.
- [45] S. Tongay, H. Sahin, C. Ko, A. Luce, W. Fan, K. Liu, J. Zhou, Y.-S. Huang, C.-H. Ho, J. Yan, D. F. Ogletree, S. Aloni, J. Ji, S. Li, J. Li, F. M. Peeters, J. Wu, *Nat. Commun.* **2014**, *5*, 3252.
- [46] H. Li, Q. Zhang, C. C. R. Yap, B. K. Tay, T. H. T. Edwin, A. Olivier, D. Baillargeat, *Adv. Funct. Mater.* **2012**, *22*, 1385.
- [47] C. Lee, H. Yan, L. E. Brus, T. F. Heinz, J. Hone, S. Ryu, *ACS Nano* **2010**, *4*, 2695.
- [48] A. Berkdemir, H. R. Gutierrez, A. R. Botello-Mendez, N. Perea-Lopez, A. L. Elias, C. I. Chia, B. Wang, V. H. Crespi, F. Lopez-Urias, J. C. Charlier, H. Terrones, M. Terrones, *Sci. Rep.* **2013**, *3*, 1755.
- [49] L. T. Liu, S. B. Kumar, Y. Ouyang, J. Guo, *IEEE Trans. Electron Devices* **2011**, *58*, 3042.
- [50] X. Liu, J. Hu, C. Yue, N. Della Fera, Y. Ling, Z. Mao, J. Wei, *ACS Nano* **2014**, *8*, 10396.
- [51] F. Reale, P. Palczynski, I. Amit, G. F. Jones, J. D. Mehew, A. Bacon, N. Ni, P. C. Sherrell, S. Agnoli, M. F. Craciun, S. Russo, C. Mattevi, *Sci. Rep.* **2017**, *7*, 14928.
- [52] D. S. Schulman, A. Sebastian, D. Buzzell, Y. T. Huang, A. J. Arnold, S. Das, *ACS Appl. Mater. Interfaces* **2017**, *9*, 44617.
- [53] D. Ovchinnikov, A. Allain, Y. S. Huang, D. Dumcenco, A. Kis, *ACS Nano* **2014**, *8*, 8174.

- [54] A. M. Hussain, G. Sevilla, K. R. Rader, M. M. Hussain, in *Saudi International Electronics, Communications and Photonics Conference (SIEPCP)*, Riyadh, Saudi Arabia **2013**, pp. 1–5.
- [55] M. W. Iqbal, M. Z. Iqbal, M. F. Khan, M. A. Shehzad, Y. Seo, J. H. Park, C. Hwang, J. Eom, *Sci. Rep.* **2015**, *5*, 10699.
- [56] S. E. Xie, L. J. Tu, Y. M. Han, L. J. Huang, K. Kang, K. U. Lao, P. Poddar, C. Park, D. A. Muller, R. A. DiStasio, J. Park, *Science* **2018**, *359*, 1131.
- [57] A. Y. Lu, H. Y. Zhu, J. Xiao, C. P. Chuu, Y. M. Han, M. H. Chiu, C. C. Cheng, C. W. Yang, K. H. Wei, Y. M. Yang, Y. Wang, D. Sokaras, D. Nordlund, P. D. Yang, D. A. Muller, M. Y. Chou, X. Zhang, L. J. Li, *Nat. Nanotechnol.* **2017**, *12*, 744.
- [58] Y. C. Lin, R. K. Ghosh, R. Addou, N. Lu, S. M. Eichfeld, H. Zhu, M. Y. Li, X. Peng, M. J. Kim, L. J. Li, R. M. Wallace, S. Datta, J. A. Robinson, *Nat. Commun.* **2015**, *6*, 8311.
- [59] J. M. Woods, Y. Jung, Y. J. Xie, W. Liu, Y. H. Liu, H. H. Wang, J. J. Cha, *ACS Nano* **2016**, *10*, 2004.
- [60] K. Kang, K. H. Lee, Y. M. Han, H. Gao, S. E. Xie, D. A. Muller, J. Park, *Nature* **2017**, *550*, 229.
- [61] Y. J. Gong, J. H. Lin, X. L. Wang, G. Shi, S. D. Lei, Z. Lin, X. L. Zou, G. L. Ye, R. Vajtai, B. I. Yakobson, H. Terrones, M. Terrones, B. K. Tay, J. Lou, S. T. Pantelides, Z. Liu, W. Zhou, P. M. Ajayan, *Nat. Mater.* **2014**, *13*, 1135.